Journal of Alloys and Compounds 527 (2012) 157–162

Contents lists available at SciVerse ScienceDirect

Journal of Alloys and Compounds

journal homepage: www.elsevier.com/locate/jallcom

Pyroelectric properties and electrical conductivity in samarium doped $BiFeO_3$ ceramics

Y.B. Yao[a,b], W.C. Liu[a,c], C.L. Mak[a,*]

[a] Department of Applied Physics, The Hong Kong Polytechnic University, Hung Hom, Kowloon, Hong Kong SAR, China
[b] Advanced Nanofabrication, Imaging and Characterization Core Lab, King Abdullah University of Science and Technology, Thuwal, Jeddah, Saudi Arabia
[c] National Laboratory of Solid State Microstructures and School of Modern Engineering and Applied Sciences, Nanjing University, Nanjing 210093, China

ARTICLE INFO

Article history:
Received 13 December 2011
Accepted 29 February 2012
Available online xxx

Keywords:
$BiFeO_3$
Pyroelectric
Sm^{3+} doping

ABSTRACT

Samarium (Sm^{3+}) doped $BiFeO_3$ (BFO) ceramics were prepared by a modified solid-state-reaction method which adopted a rapid heating as well as cooling during the sintering process. The pyroelectric coefficient increased from 93 to 137 $\mu C/m^2$ K as the Sm^{3+} doping level increased from 1 mol% to 8 mol%. Temperature dependence of the pyroelectric coefficient showed an abrupt decrease above 80 °C in all samples, which was associated with the increase of electrical conductivity with temperature. This electrical conduction was attributed to oxygen vacancy existing in the samples. An activation energy of ~0.7 eV for the conduction process was found to be irrespective of the Sm^{3+} doping level. On the other hand, the magnetic Néel temperature (T_N) decreased with increasing Sm^{3+} doping level. On the basis of our results, the effects of Sm doping level on the pyroelectric and electrical properties of the BFO were revealed.

1. Introduction

Magnetoelectrics are the class of materials exhibiting coexistence of magnetic and ferroelectric ordering in a certain temperature range. These materials have large potential for applications in magnetic as well as ferroelectric devices. Bismuth ferrite (BFO) compound is one of the very few known magnetoelectric systems with a strong linear coupling term. It exhibits antiferromagnetic ordering with high Néel temperature ($T_N \sim 370$ °C) and ferroelectric behavior with high ferroelectric Curie temperature ($T_C \sim 830$ °C) [1]. Despite possessing a high T_C, bulk BFO exhibits weak ferroelectric behavior, i.e. the remnant polarization (P_r) is as small as ~3.5 $\mu C/cm^2$ [2]. Recently, a large P_r (90–100 $\mu C/cm^2$) has been observed in BFO thin films as well as single crystals at room temperature [1,3], which is consistent with the theoretical predictions [4]. New processing techniques have been developed to synthesize single-phase BFO ceramics, and the most famous one is rapid liquid phase sintering (RLPS). In RLPS method, a single-step firing approach was adopted: the green ceramic samples were heated to the sintering temperature (~855 °C) with an extremely high heating rate ~100 °C/s. After soaking for a short period of time, the samples were cooled down to room temperature quickly [5,6]. Such high heating rate is only feasible by using a rapid thermal furnace, and the dimensions of the samples are limited if one considers the thermal equilibrium in the samples. In the present work, a simple modified conventional solid-state-reaction method was proposed to prepare BFO ceramics.

In order to improve the electrical and magnetic properties of BFO, several types of element have been used to substitute the A-site Bi^{3+} ions, for example, rare-earth type (Y^{3+}, La^{3+}, Nd^{3+}, Sm^{3+}, Gd^{3+} and Yb^{3+}) or alkali earth type (Sr^{2+}, Ba^{2+} and Ca^{2+}) [5–10]. Through doping, the leakage current density is reduced and the ferroelectric as well as magnetic properties are also improved to some extends [5–10]. However, limited reports have been dedicated to study the effects of doping on their pyroelectric properties [6,11–14].

As a good pyroelectric material, it should possess large pyroelectric coefficient, high resistivity, small dielectric permittivity and low thermal capacity [15]. BFO bears many virtues for pyroelectric applications, such as, low dielectric permittivity (~100), large ferroelectric polarization (~90–100 $\mu C/cm^2$) and high Curie temperature (~830 °C) [1–6]. Reasonable pyroelectric coefficients of ~30 and ~15 $\mu C/m^2$ K were reported for BFO ceramics and thin films at room temperature, respectively [6,11]. Shaldin et al. investigated the pyroelectric properties of BFO crystal at low temperature, ranging from 4.2 to 200 K. However, they found it was difficult to investigate their ferroelectric properties at high temperature because of the high conductivity of BFO at $T > 200$ K [12]. In this paper, we studied the effects of Sm doping on the pyroelectric and dielectric properties as well as electrical conductivity of the BFO ceramics.

2. Experimental

Stoichiometric amounts of high purity Bi_2O_3 (99.9%) and Fe_2O_3 (99.9%), together with Sm_2O_3 oxides (99.9%), were weighed and ball-milled in ethanol for 24 h. The Sm

* Corresponding author.
E-mail address: apaclmak@polyu.edu.hk (C.L. Mak).

0925-8388/$ – see front matter © 2012 Elsevier B.V. All rights reserved.
doi:10.1016/j.jallcom.2012.02.182

doping levels were fixed at 1 mol%, 3 mol%, 5 mol% and 8 mol% (denoted as samples Sm1, Sm3, Sm5 and Sm8 hereafter). After ball milling, the mixture was calcined at 650 °C (T_{cal}) for 5 h in air. The calcined powders were then grounded and ball-milled again for another 48 h. Polyvinyl alcohol was added into the dried powders as a binder. The powders were uniaxially pressed at 200 MPa into disks with a diameter of 10 mm. After burning the binder at T_{cal} for another 2 h, the samples underwent sintering. The sintering temperature (T_{sin}) was fixed at 835 °C. For the sintering process, we adopted a higher heating as well as cooling rate (heating: 30 °C/min, cooling: 100 °C/min) than the conventional solid-state-reaction method (~2 °C/min). In order to get the high cooling rate, the furnace door was opened as soon as the sintering process had finished.

X-ray diffractometer (X'pert System, Philips) with a Cu K_α source operated at an acceleration voltage of 50 kV was used to study the crystallographic phase of the samples. Raman spectra were taken at room temperature using 488 nm laser line of an air cooled Ar-ion laser. A microscope was used to focus the incident laser beam to a spot of about 100 μm in diameter. Raman spectra were recorded by a 100X objective lens in a back scattering geometry using a Raman spectrometer (Horiba Jobin Yvon, HR800) equipped with a charge coupled device. The samples were mounted on a heating stage with temperatures varied between 25 °C and 150 °C. For electrical measurements, the samples were thinned to ~0.3 mm in thickness. Silver electrodes (2 mm in diameter) were formed on both sides of the disk using screen printing method. The dielectric properties were measured on an HP4294A impedance analyzer at frequencies from 1 kHz to 1 MHz with temperatures varying from 25 °C to 450 °C. Before performing the pyroelectric measurement, the samples were poled in a silicon oil bath at 110 °C for 12 h and then slowly cooled to room temperature under field. Since the samples were apt to break down under high electrical field due to the electrical leakage, a low electrical field just above the coercive field and a prolonged duration were adopted. After poling, the samples were placed into a short-circuit state overnight to eliminate the surface charges. Pyroelectric measurements were carried out at temperatures varying from 25 °C to 110 °C at 10 MHz. The details of the pyroelectric measurements using dynamic method were described elsewhere [16]. The piezoelectric coefficient (d_{33}) of the polarized samples was measured using a piezo-d_{33} meter (YE2730A d_{33} meter, SINOCERA). Low frequency ac electrical conductivity and dielectric permittivity of the poled samples was taken on a computer-controlled lock-in amplifier (SR850, SRS Co.) at frequencies ranging from 2 MHz to 100 kHz with temperatures range between 25 °C and 180 °C.

3. Results and discussion

Fig. 1 shows the XRD patterns of pure and 5% Sm doped BFO ceramics. The major peaks were indexed as $BiFeO_3$. The XRD results also suggested the formation of small amount second phase ($Bi_{25}FeO_{39}$). The approximate fraction of BFO phase in the samples was determined from the XRD peak intensities using the relation: BFO% ≈ I_{max}(BFO)/[I_{max}(BFO) + I_{max}(second phase)]. The phase purity was found to be 90–92% for all samples. This was attributed to a loss of the volatile bismuth during the calcinations process [17]. Fig. 1(b) illustrates that pure BFO ceramic shows two clear peaks corresponding to (1 0 4) and (1 1 0) peaks, while in Sm doped BFO, these two peaks show a trend to coalescence and form a broad peak. These phenomena indicate that there is a trend to transform from rhombohedral phase to tetragonal phase in BFO ceramics due to Sm substitution [18].

At high electrical field and high temperature the BFO ceramics are apt to break down [19], therefore, the poling field and the poling temperature of all the samples were set at 70 kV/cm and room temperature, respectively. This poling field value was slightly larger than the E_c ~ 56 kV/cm obtained in our samples. Fig. 2(a) shows the typical poling-time dependence of pyroelectric coefficient (p) and piezoelectric coefficient (d_{33}) of the Sm-doped BFO samples. The p and d_{33} considerably increased with the poling time, especially in the samples poled for less than 12 h. For samples with poling time longer than 12 h, both the pyroelectric and piezoelectric coefficients were found to be saturated. Therefore, all the samples were poled for 24 h. The obtained pyroelectric and piezoelectric coefficients were 93, 87, 112, and 137 μC/m^2 K, and 47, 52, 53, and 54 pC/N for Sm1, Sm3, Sm5 and Sm8 samples, respectively. Obviously, samples with higher Sm doping level exhibited larger pyroelectric and piezoelectric coefficients. The measured pyroelectric coefficients of all the samples as a function of temperature are shown in Fig. 2(b). For low Sm doping level, the pyroelectric coefficient slightly increased with temperature and then reached a maximum at about 80 °C. Afterwards, the pyroelectric coefficient decreased as temperature further increased. On the other hand, for high Sm doping level, the pyroelectric coefficient remained constant at low temperature and decreased as temperature increased above 80 °C. It is worth to note that an abrupt decrease above ~80 °C was observed in all the curves (marked with an arrow in Fig. 2(b)). Decrease of pyroelectric coefficient is usually due to the depolarization effect at temperatures above ferroelectric transition temperature [20]. However, in current case, the samples were unlikely to be depolarized since the curve of temperature dependence of pyroelectric coefficients measured in heating process and cooling process coincided with each other. In order to clarify whether a phase transition exists in the temperature range (~80 °C), both temperature dependence of Raman spectroscopy and dielectric measurements were carried out.

Fig. 3(a) and (b) show the temperature dependence curves of the dielectric permittivity (ε_r) and loss ($\tan\delta$) measured at 10 kHz, 100 kHz and 1 MHz for sample Sm1. A very diffuse dielectric anomaly was observed in the ε_r–T curve around 250–450 °C. The peak temperature increased significantly with increasing measurement frequency, reflecting a strong frequency dispersion feature. Similar phenomenon was also observed for other Sm-doped BFO samples. Fig. 4(c) and (d) show the temperature dependence of ε_r and $\tan\delta$ of all the samples measured at 100 kHz, respectively. The positions of the dielectric anomaly for samples Sm1, Sm3, Sm5 and Sm8 were 380, 371, 335 and 338 °C, respectively. Increasing Sm content was accompanied by an obviously decreased peak position and increased dielectric maximum (ε_m). This anomaly is closely related to antiferromagnetic ordering temperature T_N ~ 370 °C. Similar dielectric anomaly has also been reported in undoped and doped $BiFeO_3$ materials [21,22]. This type of dielectric anomaly is predicted by the Landau–Devonshire theory of phase transition in magnetoelectrically ordered systems as an influence of vanishing magnetic order on the electric order [23]. No dielectric anomaly was observed around 80 °C.

Fig. 4 presents the Raman spectra of Sm-doped BFO ceramics from room temperature up to 150 °C. The Raman active modes of the rhombohedral BFO with R3c structure are summarized using the irreducible representation $\Gamma_{Raman,R3c} = 4A_1 + 9E$ [17–20]. For example, in sample Sm1, three A_1 (A_1(LO1) = 130 cm^{-1}, A_1(LO2) = 167 cm^{-1}, and A_1(LO3) = 218 cm^{-1}) and five E (E(TO1) = 79 cm^{-1}, E(TO2) = 101 cm^{-1}, E(TO7) = 482 cm^{-1}, E(TO8) = 527 cm^{-1}, E(TO9) = 600 cm^{-1}) phonon modes were identified. The shoulders around 260 cm^{-1} and 340 cm^{-1} were assigned as the E modes (E(TO3–6): 255–321 cm^{-1}) [24–27]. The A_1(LO4) mode around 425–490 cm^{-1} was not observed. The slight difference in some of the peaks position observed by different authors can be attributed to different preparation process. Figs. 3(d) and 4(b) present the detailed views for some bands where the strongest anomaly was observed in the corresponding samples. The temperature evolution of the deconvoluted peak positions and widths of A_1(LO1) and A_1(LO2) modes are illustrated in Fig. 3(e) and (f) for samples Sm1 and Sm3 respectively. With increasing temperature, the phonon modes generally decreased in intensity, shifted to lower frequency and became broadened because of anharmonic effects of the lattice. Such trends agree with previous investigations in undoped BFO materials [24,26]. It is noticed that the phonon anomaly is very prominent for the A_1(LO2) band around 167 cm^{-1} (marked with an arrow). The A_1(LO2) mode in sample Sm1 was lowered from 167 cm^{-1} to 148 cm^{-1} and broadened from 18 cm^{-1} to 69 cm^{-1} as temperature increased from 35 °C to 140 °C. In sample Sm3 the mode was lowered from 166 cm^{-1} to 154 cm^{-1} and broadened from 26 cm^{-1} to 52 cm^{-1} as temperature increased from 25 °C to 150 °C.

The peak assignments for the Raman spectra were basically the same at different temperatures ranging from room temperature

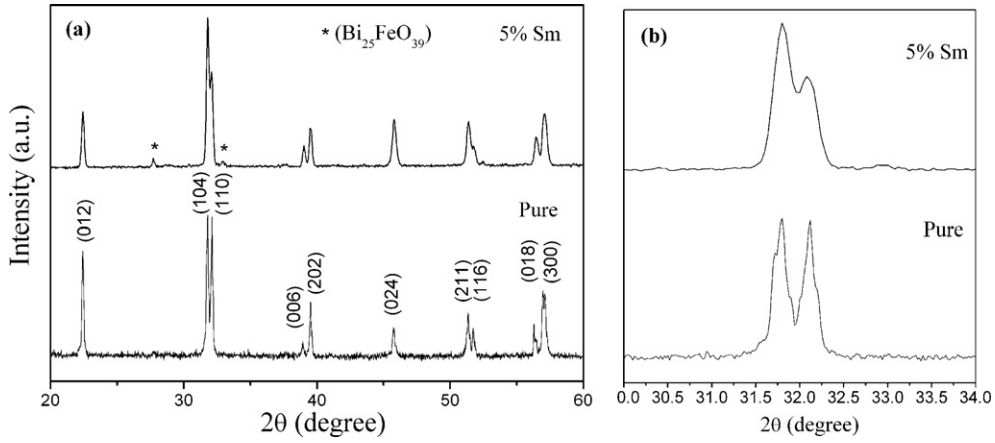

Fig. 1. (a) XRD patterns of pure and 5% Sm doped BFO ceramics; (b) enlarged (1 0 4) peaks.

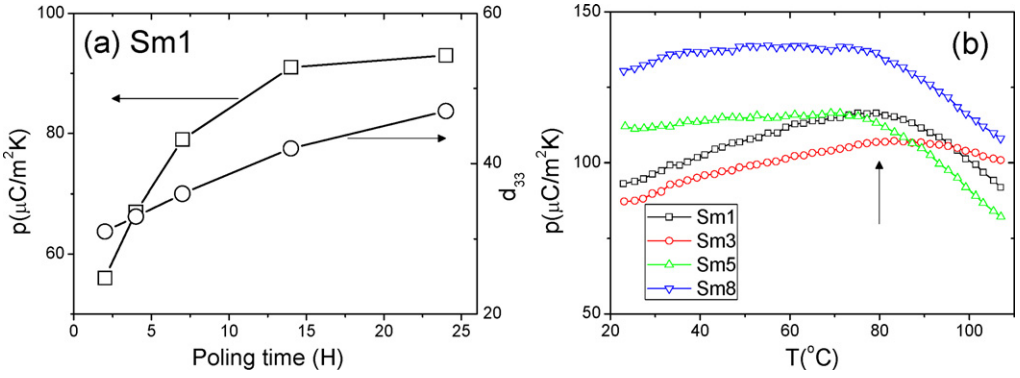

Fig. 2. (a) Poling time effects on the pyroelectric coefficient (p) piezoelectric coefficient (d_{33}) of Sm1 sample; (b) temperature (T) dependence of p of the BFO ceramics with different Sm doping concentrations.

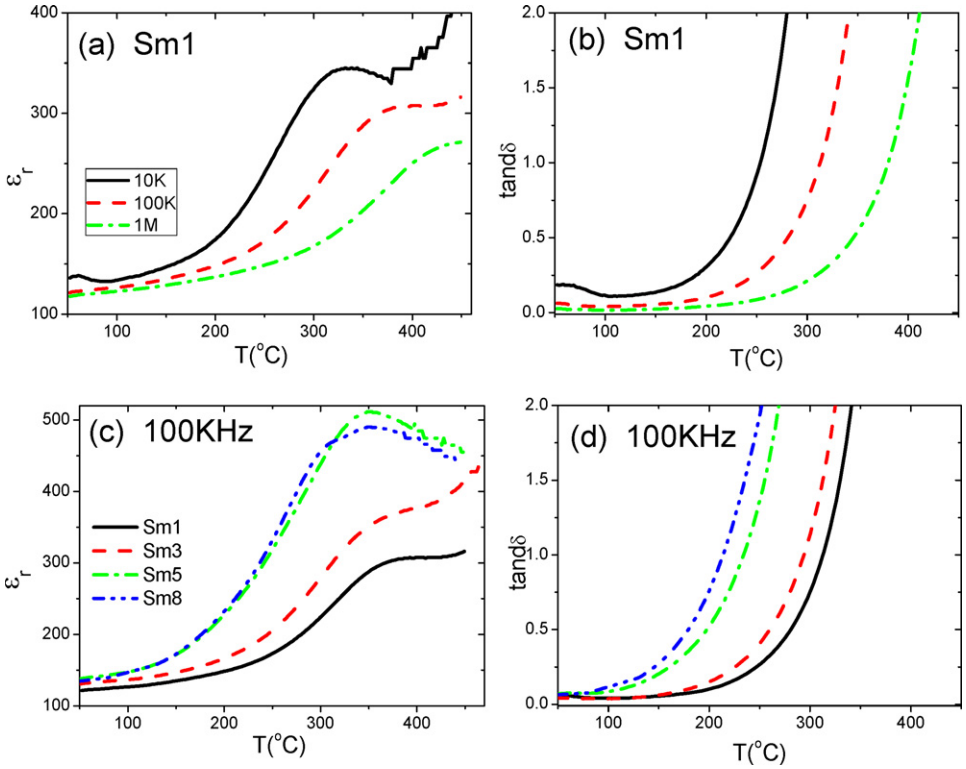

Fig. 3. Temperature dependence (T) of (a) relative dielectric permittivity ε_r and (b) dielectric loss tan δ at different frequencies of Sm1 sample; (c) relative dielectric permittivity ε_r and (b) dielectric loss tan δ at 100 kHz of BFO ceramics with different Sm doping concentrations.

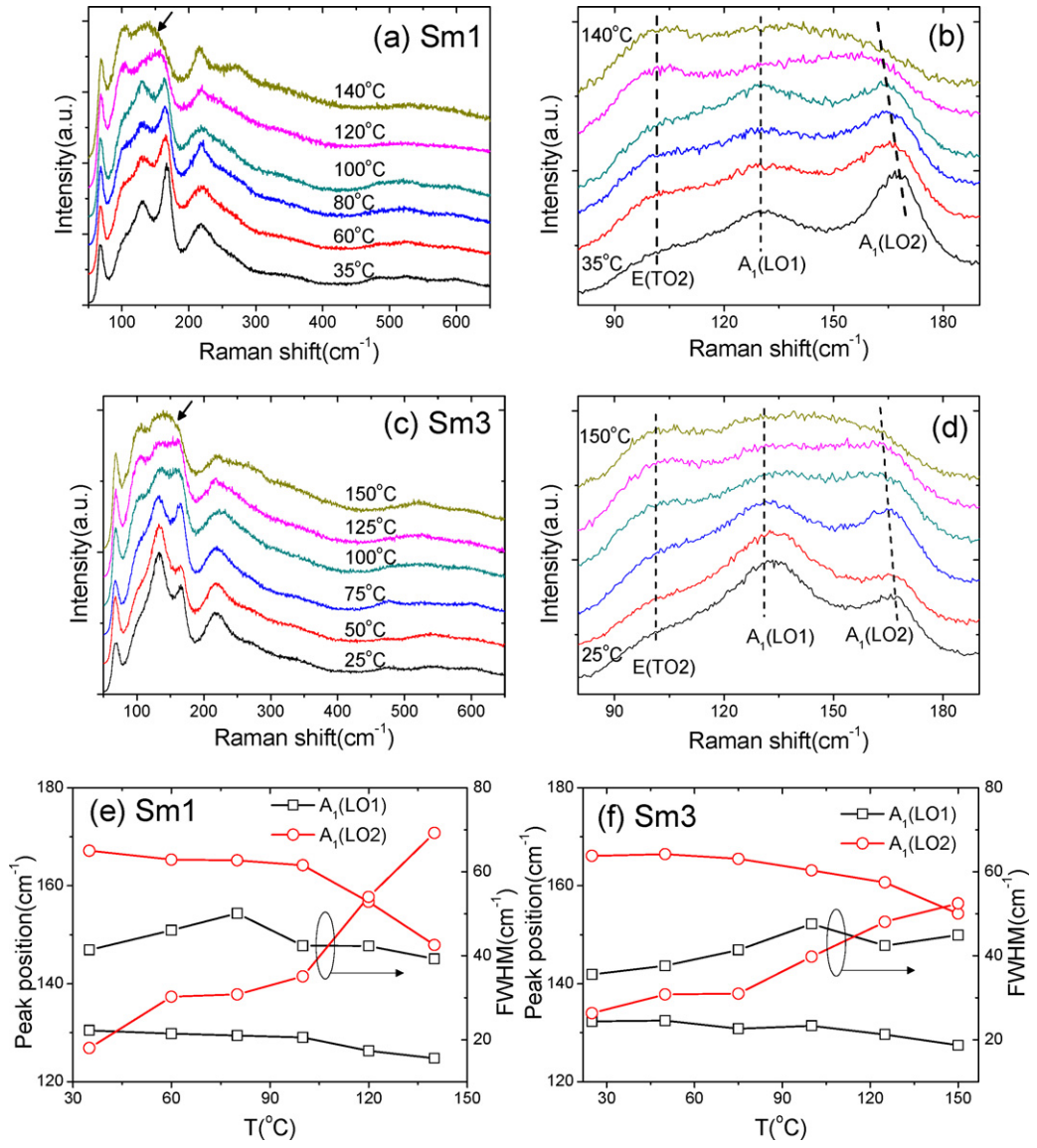

Fig. 4. Temperature-dependent evolution of Raman spectra in (a) Sm1 and (c) Sm3 samples; the enlarged views of the major bands around 80–190 cm^{-1} of (b) Sm1 and (d) Sm3 samples. Temperature evolution of the peak positions and FWHMs of A_1(LO1) and A_1(LO2) modes in (e) Sm1 and (f) Sm3 samples.

to 150 °C. Indeed, only the peak generally decreased in intensity and became broadened, while their peak positions shifted to lower frequency. This behavior was mainly due to anharmonic effects of the lattice and possibly not related to any phase transition. Therefore, we believe that the possibility of ferroelectric phase transition existed at ~80 °C is not likely to be happened. Furthermore, previous studies also ruled out the possibility of a magnetic phase transition existed at ~80 °C [24,26]. Actually, the broadening and shifting to low wavenumber of the bands with increasing temperature are explained by thermal expansion and thermal disorder, respectively [26]. Strong electron–phonon coupling where the free carriers (or polarons) contribute in an important manner to the effective force constant was reported in other magnetic oxides, such as $SrRuO_3$ [28], $A_2Mn_2O_7$ (A = Tl, In, Y) [29], and $La_{0.7}Ca_{0.3}MnO_3$ [30]. The electrical conductivity of the BFO ceramics increases with temperature considerably, which will be shown in the following section. Therefore such coupling could be another source for these phonon anomalies and further study will be needed before a conclusive remark can be reached.

Fig. 5(a) and (b) show the frequency dependence of the dielectric permittivity for samples Sm1 and Sm8 performed at temperatures varying from 25 °C to 175 °C in a wide frequency range ranging from 2 MHz to 100 kHz. For both samples, at low frequencies (below 10 Hz) and high temperatures (above 85 °C) ε' values are very large (>1000), and then drop abruptly to lower values (~100) at high frequencies. The imaginary part of dielectric permittivity (ε'') exhibits similar behavior, as shown in the inset of Fig. 5(a). Here, ε'' is larger than ε' at low frequencies and high temperatures, indicating a dc electric conduction contribution [31].

Fig. 5(c) and (d) show the frequency dependence of the real part of conductivity (σ') for samples Sm1 and Sm8 at different temperatures, respectively. At low frequencies, a constant conductivity (σ_{dc}), attributed to dc conductivity, is observed at most of the conductivity curves at different temperatures; at high frequencies, σ' increases with frequency. The conductivity is described by Jonscher universal power law: $\sigma = \sigma_{dc} + A\omega^n$ [30], where A is a constant and ω is the angular frequency. The fractional exponent n is often used to describe the ac component contributing to the dispersive region and is roughly treated to be a constant less than 1. By fitting the data,

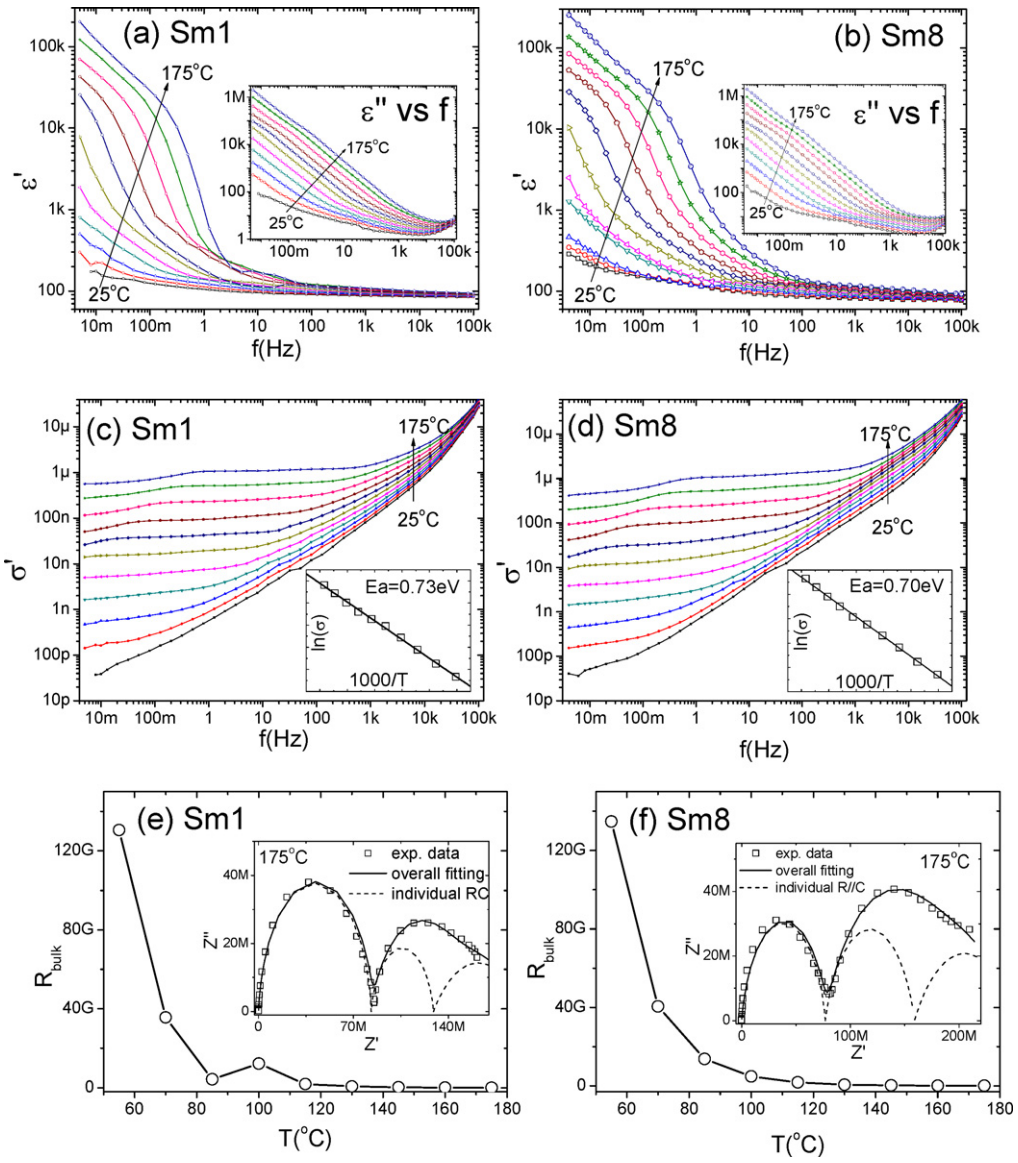

Fig. 5. Frequency dependence of the real part of the relative dielectric permittivity ε', electrical conductivity σ' of Sm1 (a, c) and Sm8 (c, d) samples under different temperatures; temperature evolution of the bulk resistance R_{bulk} in (e) Sm1 and (f) Sm8 samples. The insets in figure (a) and (b) show the frequency dependence of imaginary part of the relative dielectric permittivity ε'' under different temperatures. The inset in figure (c) and (d) illustrate the Arrhenius plots of the dc conductivity σ_{dc}. The insets in figure (e) and (f) depict the Cole–Cole plots of the complex impedance Z^* and the data were fitted as three R//C elements serially connected.

dc conductivities at different temperatures were obtained. And the activation energy for the dc conductivity was calculated by using the Arrhenius equation [30,31]:

$$\sigma_{dc} = \sigma_0 \exp\left(-\frac{E_a}{k_B T}\right)$$

Here, E_a is the activation energy for conduction, k_B is the Boltzmann constant and T is the absolute temperature. The activation energies were found to be 0.73 eV and 0.70 eV for samples Sm1 and Sm8, respectively, as shown in the insets of Fig. 5(c) and (d). These activation energies are consistent with the barrier energy for thermal movement of oxygen vacancies [30–32].

The grain (or 'bulk') resistances (R_{bulk}) variations with temperature are shown in Fig. 5(e) and (f) for samples Sm1 and Sm8, respectively. The grain resistance was obtained by fitting the complex impedance plot (Z'' vs. Z'). A complex Cole–Cole plot was plotted for the results measured at 175 °C, as shown in the inset of Fig. 5(e) for sample Sm1. For the impedance complex plot, the semicircle dominant at the lowest frequency is usually attributed to the electrode, that at the highest frequency to the bulk grain and that at middle frequencies to the grain boundaries [32]. In our cases, two semicircles were clearly identified. However, the low-f semicircle (the larger one) is seriously deformed and can be considered as two semicircles superposed. The complex plot was fitted by modeling the sample as an equivalent circuit of three R//C elements connected serially (corresponding to the grain, grain boundary, and electrode interface, respectively):

$$Z^* = \frac{R_1}{1+(j\omega R_1 C_1)^{\alpha 1}} + \frac{R_2}{1+(j\omega R_2 C_2)^{\alpha 2}} + \frac{R_3}{1+(j\omega R_3 C_3)^{\alpha 3}},$$

where $0 < \alpha < 1$ and $\alpha = 1$ denotes ideal Debye condition [33], $R_1//C_1$: grain, $R_2//C_2$: grain boundary, $R_3//C_3$: electrode interface. The fitting curve is shown in the inset of Fig. 5(a). The fitting parameters are: 83 MΩ/6 pF (R_1/C_1), 46 MΩ/8.5 nF (R_2/C_2) and 66 MΩ/120 nF (R_3/C_3). The α values were found to be 0.94, 0.87 and 0.52 for grain, grain boundary and electrode interface, respectively. The bulk resistance of sample Sm1 decreased abruptly from 483 GΩ at 40 °C to

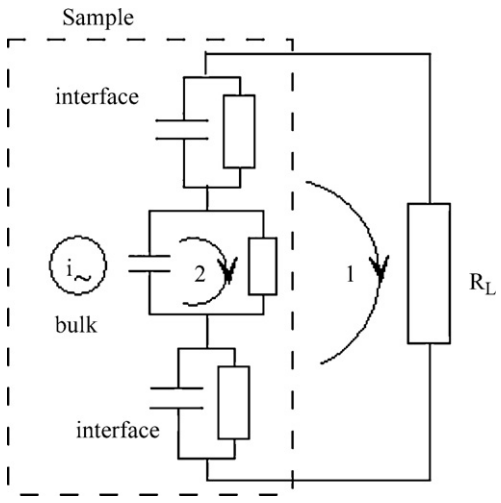

Fig. 6. Electrical model for temperature dependence of the pyroelectric coefficients.

18 GΩ at 85 °C, as shown in Fig. 5(e). Similar trends were observed in other samples, as shown in Fig. 5(f) for sample Sm8.

In order to explain the temperature dependence of the pyroelectric properties of the samples, we use a serial R//C element model as shown in Fig. 6. Here, we consider the Sm doped BFO sample to be three R//C elements in series, corresponding to bulk (grain) and interface (grain boundary and electrode interface). The capacitor of the bulk element acts as a current source. The pyroelectric current is detected through a load resistor (R_L) and the current normally goes through loop '1', as indicated in Fig. 6. Apart from this normal current, another possible path for the pyroelectric current is inside the bulk element indicated as loop '2' in the figure. The smaller the resistance R, the larger the proportion of the pyroelectric current present inside loop '2'. Since a drastic decrease of the resistance of the bulk element was observed as previously discussed (Fig. 5(e) and (f)), more pyroelectirc current will go through the loop '2' at higher temperatures. Therefore, the pyroelectric current probed by the external circuit (R_L) is decreased and so is the measured pyroelectric coefficient. The microscopic scenario for this process is that at higher temperatures the pyroelectric charge is compensated by the thermally-activated mobile charge carriers inside the grain.

4. Conclusions

In summary, samarium (Sm^{3+}) doped $BiFeO_3$ (BFO) ceramics were prepared by a modified solid-state-reaction method which adopted a higher heating as well as cooling rate during the sintering process. The samples were fully poled at a low electrical field ($\sim E_c$) for over 20 h. The pyroelectric and piezoelectric coefficients at room temperature were 93, 87, 112, and 137 μC/m^2 K, and 47, 52, 53, and 54 pC/N for samples Sm1, Sm3, Sm5 and Sm8, respectively. The pyroelectric coefficients decreased at $T > 80$ °C in all samples, which was found to be related with the decrease of grain resistance. The activation energy (~0.7 eV) for the electrical conduction process was found to be irrespective of compositions. Oxygen vacancy is responsible for the electrical conduction. After Sm doping, the magnetic Néel temperature (T_N) was decreased from 380 °C in Sm1 to 338 °C in Sm8 sample.

Acknowledgement

This work was supported by the Hong Kong Polytechnic University under Grant No. GYH08.

References

[1] J. Wang, J.B. Neaton, H. Zheng, V. Nagarajan, S.B. Ogale, B. Liu, D. Viehland, V. Vaithyanathan, D.G. Schlom, U.V. Waghmare, N.A. Spaldin, K.M. Rabe, M. Wuttig, R. Ramesh, Science 299 (2003) 1719.
[2] J.R. Teague, R. Gerson, W.J. James, Solid State Commun. 8 (1970) 1073.
[3] D. Lebeugle, D. Colson, A. Forget, M. Viret, Appl. Phys. Lett. 91 (2007) 022907.
[4] J.B. Neaton, C. Ederer, U.V. Waghmare, N.A. Spaldin, K.M. Rabe, Phys. Rev. B 71 (2005) 014113.
[5] G.L. Yuan, S.W. Or, H.L.W. Chan, J. Phys. D: Appl. Phys. 40 (2007) 1196.
[6] G.L. Yuan, S.W. Or, Appl. Phys. Lett. 88 (2006) 062905.
[7] V.A. Khomchenko, D.A. Kiselev, J.M. Viera, L. Jian, A.L. Kholkin, A.M.L. Lopes, Y.G. Pogorelov, J.P. Araujo, M. Maglione, J. Appl. Phys. 103 (2008) 024105.
[8] S. Fujino, M. Murakami, V. Anhusathaiah, S.H. Lim, V. Nagarajan, C.J. Fennie, M. Wuttig, L. Salamanca-Riba, I. Takeuchi, Appl. Phys. Lett. 92 (2008) 202904.
[9] Z. Yan, K.F. Wang, J.F. Qu, Y. Wang, Z.T. Song, S.L. Feng, Appl. Phys. Lett. 91 (2007) 082906.
[10] R.K. Mishra, Dillip K. Pradhan, R.N.P. Choudhary, A. Baneriee, J. Phys.: Condens. Matter 20 (2008) 045218.
[11] Y.W. Li, J.L. Sun, J. Chen, X.J. Meng, J.H. Chu, J. Cryst. Growth 285 (2005) 595.
[12] Yu.V. Shaldin, S. Matyjasik, A.A. Bush, Crystallogr. Rep. 52 (2007) 123.
[13] Y.K. Fetisov, A.A. Bush, K.E. Kamentsev, G. Srinivasan, Solid State Commun. 132 (2004) 319.
[14] J.Y. Park, J.H. Park, Y.K. Jeong, H.M. Jang, Appl. Phys. Lett. 91 (2007) 152903.
[15] S. Bauer, B. Ploss, J. Appl. Phys. 88 (1990) 6361.
[16] B. Ploss, M. Krause, IEEE Trans. Ultrason. Ferroelect. Freq. Control 54 (2007) 2479.
[17] Y.P. Wang, L. Zhou, M.F. Zhang, X.Y. Chen, J.M. Liu, Z.G. Liu, Appl. Phys. Lett. 84 (2004) 1731.
[18] Z. Wen, X. Shen, D. Wu, Q.Y. Xu, J.L. Wang, A.D. Li, Solid State Commun. 150 (2010) 2081.
[19] Y. Yao, B. Ploss, C.L. Mak, K.H. Wong, Appl. Phys. A 99 (2010) 211.
[20] M. Costache, I. Mateia, L. Pintiliea, H.V. Alexandrua, C. Berbecaru, J. Optoelectron. Adv. Mater. 3 (2001) 75.
[21] R. Mazumder, P. Sujatha Devi, D. Bhattacharya, P. Choudhury, A. Sen, M. Raja, Appl. Phys. Lett. 91 (2007) 062510.
[22] M. Kumar, K.L. Yadav, Appl. Phys. Lett. 91 (2007) 242901.
[23] L. Benguigui, Solid State Commun. 11 (1972) 825.
[24] H. Fukumura, H. Harima, K. Kisoda, M. Tamada, Y. Noguchi, M. Miyayama, J. Magn. Magn. Mater. 310 (2007) e367.
[25] D. Kothari, V. Raghavendra Reddy, V.G. Sathe, A. Gupta, A. Banerjee, A.M. Awasthi, J. Magn. Magn. Mater. 320 (2008) 548.
[26] R. Haumont, J. Kreisel, P. Bouvier, F. Hippert, Phys. Rev. B 73 (2006) 132101.
[27] P. Hermet, M. Goffinet, J. Kreisel, Ph. Ghosez, Phys. Rev. B 75 (2007) 220102(R).
[28] D. Kirillov, Y. Suzuki, L. Antognazza, K. Char, I. Bozovic, T.H. Geballe, Phys. Rev. B 51 (1995) 12825.
[29] E. Granado, P.G. Pagliuso, J.A. Sanjurjo, R. Rettori, M.A. Subramanian, S.W. Cheong, S.B. Oseroff, Phys. Rev. B 60 (1999) 6513.
[30] K.H. Kim, J.Y. Gu, H.S. Choi, G.W. Park, T.W. Noh, Phys. Rev. Lett. 77 (1996) 1877.
[31] A. Molak, M. Paluch, S. Pawlus, J. Klimontko, Z. Ujma, I. Gruszka, J. Phys. D: Appl. Phys. 38 (2005) 1450.
[32] S. Rachna, S. Bhattacharyya, S.M. Gupta, J. Phys. Chem. Solids 69 (2008) 822.
[33] K. Sambasiva Rao, D. Madhava Prasad, P. Murali Krishna, B. Tilak, K.Ch. Varadarajulu, Mater. Sci. Eng. B 133 (2006) 141.